Undrained Poroelastic Response of Sandstones to Deviatoric Stress Change[1]

David A. Lockner[2]
Sergei A. Stanchits[2]

Abstract. Deformation of porous crustal rock, through diagenesis, tectonic loading or other processes, can change pore volume and affect fluid pressure. The largest stress-induced pore pressure changes occur when fluid is trapped in pores in an 'undrained' condition. We have measured the undrained poroelastic response of two sandstones to changes in mean and deviatoric stress. Pore pressure was found to respond to mean stress σ_m in the usual manner: $\Delta p = B\Delta\sigma_m$ (B ranging from 0.4 to 0.7), nearly independent of the ambient deviatoric stress state. However, variations in deviatoric stress ($\sigma_d = (\sigma_1 - \sigma_3)/2$) at constant mean stress were also found to induce a reversible (elastic) pore pressure response to stress levels up to and exceeding 80 percent failure stress (*i.e.,* $\Delta p = \eta\Delta\sigma_d$ $|_{\sigma_m=\text{const.}}$). The coefficient η became more negative with increasing deviatoric stress level in sandstone and Ottawa sand samples. That is, η represents a dilatant response where increased deviatoric stress causes a decrease in pore pressure. The poroelastic response to deviatoric stress is explained in terms of anisotropic matrix stiffening due to closure of crack-like pore space or flattening of grain contacts at high ambient stress levels and can be important in calculations of earthquake stress transfer.

1. Introduction

The ambient stress state of a rock mass in the Earth's crust can change gradually in response to tectonic loading or rapidly due, for example, to a nearby earthquake. If these stress changes induce pore volume changes in the rock mass, the resulting compression or decompression of the pore fluid can have a significant influence on rheology, strength, earthquake nucleation, and flow of pore fluid. The largest poroelastic effects can be expected for an 'undrained' rock for which there is no significant pore fluid flow to or from the surroundings over the time interval of interest. Theoretical and numerical analyses of poroelastic response of rocks are generally based on the constitutive theory of *Biot* [1941] which predicts that for an isotropic rock, changes in pore volume, and therefore pore pressure, will only be caused by changes in mean stress ($\sigma_m = (\sigma_1 + \sigma_2 + \sigma_3)/3$) where ($\sigma_1, \sigma_2, \sigma_3$) are principal stresses [*Rice and Cleary*, 1976; *Zimmerman*, 1991; *Roeloffs*, 1996]. This analysis has led to the familiar undrained pore pressure response relation

---

[2] US Geological Survey, 345 Middlefield Rd, Menlo Park, CA 94025
ph: 650 329-4825
e-mail: dlockner@usgs.gov

$$\Delta p_u = B \Delta \sigma_m \tag{1}$$

where B is referred to as the Skempton coefficient. (Note that in this paper we will use the sign convention that compressive stresses and contractive strains are positive.) In his work on saturated clays, *Skempton* [1954] allowed for the possibility that deviatoric stress changes might also affect pore pressure. Since care must be taken in distinguishing between reversible elastic response and irreversible permanent deformation, less ambiguous measurements of poroelastic response should be obtained using rock with cohesive strength. Apparently, the first published observations of reversible pore pressure response of competent rock to changes in deviatoric stress are by *Wang* [1997] for Indiana limestone at a confining pressure of 27.6 MPa. In that study, tests at zero deviatoric stress yielded $B = 0.53$ when fit by (1). With application of axial load, both mean and deviatoric stress were increased. In this case, the best fit by (1) resulted in B of 0.34 and 0.39 for the two reported tests. This represents a remarkable change in poroelastic response for a rock under reversible loading conditions and suggested that pore volume was responding to more than simply mean stress. Wang concluded that the incorporation of a dilatational response to increased deviatoric stress provided a significantly better fit to the data. In this paper, we provide measurements of the poroelastic response of sandstones to mean and deviatoric stress changes that confirm a dilatational deviatoric stress response which is found to vary systematically with applied stress level.

2. Generalized Stress Response

Skempton [1954] proposed a linear dependence of pore pressure on mean and deviatoric stress for a triaxial loading geometry in which $\sigma_2 = \sigma_3 = P_{conf}$. Defining deviatoric stress as $\sigma_d = (\sigma_1 - \sigma_3)/2$, Skempton's undrained pore pressure response can be written

$$\Delta p_u = B \Delta \sigma_m + 2 \left(A - \frac{1}{3} \right) B \Delta \sigma_d \tag{2}$$

where A and B are the Skempton coefficients. As an alternative representation, octahedral stress [*Jaeger and Cook*, 1984] resolved on a plane inclined at equal angles to the three principal stress axes provides a convenient choice for relating poroelastic response to the first and second stress invariants I_1 and I_2. For an isotropic medium, pore pressure response should be independent of the choice of coordinate system, and should therefore be expressible in terms of the stress invariants. The octahedral stresses can be related in a simple manner to the stress invariants and would seem a useful choice for describing stress state. Octahedral normal stress is equivalent to mean stress and is proportional to I_1:

$$\sigma_{oct} = \sigma_m = \frac{1}{3} I_1. \tag{3}$$

Octahedral shear stress is given by

$$\tau_{oct} = \frac{\sqrt{2}}{3}\left[I_1^2 + 3I_2\right]^{1/2} = \sqrt{\frac{2J_2}{3}} \qquad (4)$$

where J_2 is the second invariant of stress deviation [*Jaeger and Cook*, 1984, pp. 33]. Motivated by these relations, *Henkel and Wade* [1966] proposed a more general form of equation (2):

$$\Delta p_u = B\left[\Delta\sigma_m + \frac{3A-1}{\sqrt{2}}\Delta\tau_{oct}\right]. \qquad (5)$$

The preceding comments pertain to the poroelastic response of an isotropic rock. As we will show in Sections 4.2 and 5.2, application of deviatoric stress during our measurements leads to significant anisotropy in the rock samples tested. This stress-induced anisotropy has been well-documented in measurements of compressional wave speed anisotropy and shear wave speed birefringence in laboratory samples [*Nur and Simmons*, 1969; *Bonner*, 1974; *Lockner et al.*, 1977; *Lockner et al.*, 1992]. Both the poroelastic response reported here and the stress-induced wave speed changes result from preferential closure or opening of microcracks under a non-hydrostatic stress state. In his initial analysis, *Biot* [1941] derived stress-strain relations for the elastic consolidation of a porous, isotropic medium. This theory was later extended to describe a fully anisotropic medium [*Biot*, 1955; *Biot and Willis*, 1957]. Since our results show the development of significant matrix anisotropy, this latter analysis of Biot becomes necessary. Of particular relevance to our tests is the bottom equation (49) in *Biot and Willis* [1957, pp. 598] for transverse (or radially symmetric) anisotropy which for an undrained test reduces to

$$\Delta p_u = a\left(m\Delta\sigma_1 + 2h\Delta\sigma_3\right) = a\left[(m+2h)\Delta\sigma_m + 2(m-h)\Delta\sigma_d\right] \qquad (6)$$

where a, h, and m are related to material constants. (A concise development of anisotropic poroelastic theory has recently been presented by *Cheng* [1997].) For an isotropic medium, $m = h$ and (6) reduces to (1) (*e.g.,* [*Zimmerman*, 1991; *Cheng*, 1997]). The coefficients m and h are related to the compliance of the medium in the axial and transverse directions respectively. Increasing mean stress tends to close microcracks and increase grain contact area which should decrease m and h. Thus we expect a decrease in B with increasing mean stress or confining pressure [*Zimmerman*, 1991]. An increase in deviatoric stress resulting, for example, from an increase in σ_1, should reduce m more rapidly than h. Thus we anticipate a negative undrained pore pressure response to increasing deviatoric stress.

In the most general case, an inherently anisotropic rock might be found in a random orientation relative to the ambient stress field. However, in the present study, three factors significantly simplify the analysis. First, our samples are initially isotropic, or nearly isotropic. Since anisotropy is stress-induced, principal axes of the anisotropic material properties are aligned with the applied principal stress axes. Second, as mentioned above, for a triaxial test geometry, $\sigma_2 = \sigma_3$, and only a subset of possible stress

states can be tested. As a further simplification, σ_1 remains parallel to the sample axis, so we do not need to be concerned with rotation of the stress axes during testing. Based on these considerations, we will test a relation for undrained pore pressure response of the form

$$dp_u = \frac{\partial p}{\partial \sigma_m} d\sigma_m + \frac{\partial p}{\partial \sigma_d} d\sigma_d = B d\sigma_m + \eta d\sigma_d \ . \tag{7}$$

Then, the various parameters introduced in this section are related by

$$\begin{aligned} A &= \frac{\eta}{2B} + \frac{1}{3} \\ ah &= \frac{B}{3} - \frac{\eta}{6} \\ am &= \frac{(B+\eta)}{3}. \end{aligned} \tag{8}$$

Finally, for the triaxial geometry, changes in the octahedral stresses are given by

$$\begin{aligned} \Delta\sigma_m &= \frac{1}{3}\left(\Delta\sigma_1 + 2\Delta\sigma_3\right) = \Delta\sigma_3 + \frac{2}{3}\Delta\sigma_d \\ \Delta\tau_{oct} &= \frac{\sqrt{2}}{3}\left(\Delta\sigma_1 - \Delta\sigma_3\right) = \frac{2^{3/2}}{3}\Delta\sigma_d. \end{aligned} \tag{9}$$

3. Experimental Procedure

Two fine-grained, weakly cemented, porous sandstones were tested: Berea, with 21 percent porosity and Navajo, with 22 percent porosity. Peak deviatoric strength of Berea and Navajo, at 17 MPa effective confining pressure, were 65 and 68 MPa, respectively. Additional control tests were carried out on a fine-grained porous aluminum oxide ceramic (Coors AHP99) and on a sand pack of crushed Ottawa sand. Samples were 25.4-mm-diameter cylinders. End faces were surface-ground to be flat and parallel. Samples were evacuated for approximately 20 hr and presaturated with deionized water, which was used as the pore fluid in all experiments. Basic sample characteristics and test conditions are listed in Table 1.

In a typical test run, the sample was jacketed in a 3.2-mm-wall-thickness polyurethane tube which was sealed to steel end pieces. The sample assembly was placed in the pressure vessel and a single pore pressure line was attached to an external system consisting of a pressure transducer and pressure generator (Figure 1). The pressure generator is designed to measure volume displacements to a precision of ± 0.01 mm^3 (approximately ± 0.4 microstrain pore volume) by recording the piston position with a DCDT displacement transducer. The total capacity of the pressure generator is 250 mm^3. When the pumping direction is reversed, there is a small volume change related to readjustment of the piston seal packs. To avoid this error in pore volume determination, care was taken to carry out all measurements before and after a stress step with the

pressure generator moving in the same direction. This was a tedious but necessary process to minimize measurement errors in tests that involved small volume changes. Axial load (σ_1) was measured with an internal load cell to eliminate uncertainties due to piston seal friction. Confining pressure and axial load were recorded with ±0.02 MPa precision and pore pressure to ±0.004 MPa. All parameters (pressures, volumes, etc.) were sampled and recorded at a rate of 1 sample/s. Tests were conducted at ambient confining pressures ranging from 10 to 40 MPa, deviatoric stresses from 0 to 55 MPa, and pore pressures from 2 to 4 MPa.

The observations reported here involve measuring the undrained pore pressure response to an incremental change in the stress state applied to a sample. However, because the external pore pressure system has finite volume and compliance, a change in pore pressure in the sample will lead to fluid flow into or out of the sample as pressure equilibrates with the external system. If the effective volume of the external system is comparable to the sample pore volume, the assumption of undrained response will be invalid. We solved this problem by designing a computer-generated virtual no-flow boundary condition at the sample-endplug interface. To accomplish this we performed independent calibration runs of confining pressure and pore pressure using a solid steel sample. In these calibration runs we measured the pore volume change of the external pore pressure system associated with changes in confining pressure and pore pressure. Since these volume measurements represent the response of the external pore pressure system when there is a no-flow boundary at the sample, they are exactly the corrections needed to compute the true flow across the sample-endplug interface when a porous sample is stressed. To apply the corrections, we created a virtual pore volume computer channel consisting of the direct pore volume measurement (*i.e.,* from the reading of the pore pressure generator piston position) minus the corrections determined by the pressure/volume calibrations. During a stress step test, we would control the pressure generator to maintain a constant value of this channel. For example, if the pore pressure within the sample increased following a rise in confining pressure, water would flow from the sample to the external pore pressure system, raising pore pressure in the external system and lowering the value of the virtual pore volume channel. The pressure generator would then advance, further increasing the pore pressure, until the virtual pore volume returned to zero. At this point, if the calibrations are correct, pore pressure has risen enough so that the water initially expelled from the sample has been forced back in and a no-flow boundary condition is established.

If the sample pore volume is small compared to the equivalent volume of the external pore pressure system, a condition occurs in which most of the pore pressure increase comes from adjustment of the virtual pore volume channel. Uncertainties in the calibration terms set a practical limit to the accuracy of this compensation method. We have set a limit for this study where the pressure adjustment from the virtual pore volume channel must be less than half the pressure change coming from the direct sample response. For the sample size used here, this limits us to a minimum porosity of about 5 percent. For samples with 15 to 20 percent porosity, corrections become insignificant.

A typical test sequence involved an initial set of measurements at 10, 20 and 40 MPa confining pressure and zero deviatoric stress (the loading piston was not in contact with the sample) to determine pressure dependence of the standard Skempton coefficient *B*. In the second part of the test sequence, confining pressure was adjusted to 20 MPa and

deviatoric stress was applied by advancing a piston against the end of the sample (Figure 1). At this point, one of three tests was performed. Each test involved varying a stress component by 1 to 3 MPa.

(1) Constant deviatoric stress. Axial stress and confining pressure were ramped together so that $\Delta\sigma_d = 0$. This resulted in a change $\Delta\sigma_m$ at constant τ_{oct}.

(2) Constant mean stress. Axial stress and confining pressure were ramped in opposite directions in the ratio $\Delta\sigma_1/\Delta\sigma_3 = -2$. This resulted in a change $\Delta\sigma_d$ at constant σ_m.

(3) *Constant confining pressure.* Axial stress was changed at constant confining pressure. In this case, deviatoric stress and mean stress varied in the ratio $\Delta\sigma_{dt}/\Delta\sigma_m = 3/2$.

When the test sequence was completed, axial load was increased by 10 to 20 MPa and a new test sequence was performed. This procedure was repeated at increasing ambient deviatoric stress level until approximately 80 percent failure stress. At this point, the natural time-dependent creep associated with sample failure was so rapid that it became impossible to maintain constant pore pressure. It should be noted that at each ambient stress level, stress steps were repeated, both forwards and backwards two to four times to test for reversibility of the pore pressure response. Especially at the higher deviatoric stress levels, the first stress step that moved the sample closer to failure would produce a measurable inelastic strain component. While the pore pressure response of this first stress step would not be reproducible, repeated cycles of stress steps would lead to a reproducible response. In subsequent sections we generally distinguish between pore pressure response involving permanent deformation and response that is reversible.

A representative test sequence at 15 MPa deviatoric stress is shown in Figure 2. Control variables are confining pressure and deviatoric stress (Figure 2a) and pore volume change (Figure 2b). Pore pressure response, also shown in the lower plot, is the dependent variable. Pore volume is the virtual control channel described above that corrects for the external system compressibility and represents the volume of water flowing into the sample. Note the slow, steady increase in P_{vol} at a rate of 0.003 cm^3/hr. As described above, this constant increase guaranteed that the pump was steadily advancing during the measurements to eliminate pore volume uncertainties related to pump backlash characteristics. At decreasing pore pressure steps (*i.e.,* 900 and 1030 sec), the pump would have to reverse direction momentarily. We adopted the procedure that at decreasing pore pressure steps we would manually run the pump backwards so that the pump would then move forward under computer control to come back to the pore volume set point. As shown in Figure 2b, this process would take one to two minutes to complete. Thus, all pore pressure measurements were made with the pump advancing and at the pore volume set point. Because of the steady advance of the pump, pore pressure in the sample also steadily increased as shown in Figure 2b. Pore pressure data were therefore de-trended before determination of the pore pressure response to stress steps.

The first test sequence (indicated by '*i*' in Figure 2a) involved two steps up and two steps down in confining pressure. Each 1.0 MPa confining pressure step resulted in approximately 0.5 MPa change in pore pressure. This yields $B = \sim0.5$. The second test sequence, labeled '*ii*', involved a 1.5 MPa change in deviatoric stress at constant confining pressure. Pore pressure response in this case was approximately 0.3 MPa. Since both shear and mean stress varied together in this test, η and B cannot be determined independently (see above). This measurement is used later to test the validity of (7). The final test sequence '*iii*' involved changes in confining pressure and deviatoric stress to

vary shear stress while maintaining constant mean stress. In this case, the pore pressure response of approximately 0.3 MPa implies $\eta \sim$ -0.1. This value corresponds to a Skempton coefficient (equation (2)) of $A \sim$ 0.23 which is similar to the values reported for limestone [*Wang*, 1997].

Uncertainties in determinations of the poroelastic coefficients η and B come from a variety of sources. A significant potential error, especially at higher deviatoric stress, is the inclusion of inelastic volumetric strain in the response to an incremental stress step. In general, this inelastic strain increment will occur during the first increasing stress increment at a given stress level. We eliminated this error source by carrying out repeated measurements (by cycling stress steps up and down) until repeatable results were obtained. Generally, only the first increasing stress increment showed a component of irreversible strain. These first stress steps are shown as open symbols in the data plots and have not be used in estimates of η and B. At the highest deviatoric stress levels, samples were undergoing steady creep and it became impossible to obtain repeatable results. Therefore, we do not report estimates for the poroelastic coefficients above 80 percent failure stress. When samples were tested in the elastic regime, accuracy in determining η and B depended on sample porosity, sample matrix stiffness and the magnitude of the applied stress increment. The poroelastic response of the sandstones was found to be non-linear over a wide range in applied stress. To determine the locally linear response as represented by equation (7), we restricted stress perturbation increments to less than 3 MPa. Repeatability in determining η and B was then determined by cycling stress up and down and computing standard deviation. A typical 2-sigma error for the sandstones and Ottawa sand pack was ±0.02. As a further test of measurement repeatability, two separate Berea samples were tested under similar deviatoric stress conditions. The samples gave identical results to within the measurement accuracy just stated.

4. Results

4.1. Hydrostatic tests

The first sequence of tests were conducted as a function of confining pressure without application of deviatoric stress (no piston contact with the sample). Measurements were made at nominal confining pressure and therefore mean stress of 10, 20, and 40 MPa. Pore pressure was kept within a range of 2 to 4 MPa, resulting in nominal effective confining pressure of 7, 17 and 37 MPa. Confining pressure steps of 1 and 2 MPa, both increasing and decreasing, were applied repeatedly at each ambient pressure level. Results for the two sandstones and the Ottawa sand pack are shown in Figure 3. Each data point represents pore pressure response to a single confining pressure step as shown in Figure 2. Open symbols represent the first test at a given confining pressure. Solid symbols indicate second, third and forth determinations. We found, especially at higher pressures, that the first test involved a component of permanent strain and often gave a pore pressure response that differed significantly from subsequent test steps. Since we claim to be measuring elastic (reversible) response, these open symbol measurements should be regarded with caution. This also shows the importance of performing cyclic measurements rather than a single ramp in stress, since porous materials may undergo significant inelastic deformation when first loaded, even at relatively low stress levels.

Trends for the three samples in Figure 3 are indicated by dashed lines. All three samples show a general decrease in pore pressure response with increasing confining pressure. The two sandstones show similar pressure dependence, with *B* dropping to ~0.4 by 40 MPa effective confining pressure. Values for Berea, reported by *Green and Wang* [1986] at lower confining pressure are also plotted. Combined with our measurements, these provide a complete undrained pore pressure response for Berea from zero to 40 MPa effective confining pressure. The most rapid decrease in *B* (more than 40 percent) occurs in the first 20 MPa of confining pressure. The sand pack, with no cohesion or grain cementation, is more porous and forms a more compliant grain matrix than the sandstones. As a result, the sand pack has a larger Skempton coefficient consistent with comments following equation (6). The large value (*B* = 0.87) for sand at 37 MPa effective confining pressure represents a pore pressure increase during the first 1 MPa confining pressure step that included a significant irreversible matrix compaction component. Subsequent measurements (*B* = 0.68) show the reversible elastic component of deformation.

4.2. Deviatoric stress tests.

A suite of five samples were tested under non-hydrostatic stress conditions to determine the sensitivity of pore pressure response to both mean and deviatoric stress perturbations. All tests were conducted at a nominal confining pressure of 20 MPa and pore pressure from 2 to 4 MPa. Deviatoric stress levels as high as 55 MPa were applied. Since tests were carried out at constant confining pressure, the applied mean stress increased over a full test cycle from 20 MPa to as much as 57 MPa. In future tests, we intend to map out the poroelastic response to a broader range of stress states. Results from two Berea sandstone tests are shown in Figure 4 where poroelastic coefficients η and *B* are plotted as a function of deviatoric stress. That is, tests were performed at successively higher deviatoric stress levels. At each stress level, pore pressure response was observed for changes in mean and deviatoric stress levels of up to 3 MPa (see description in Section 3). Open symbols show response to the first stress step. Solid symbols show response to subsequent steps involving repeated cycling of stress. The average value of *B* (mean stress sensitivity) ranges from 0.45 to 0.50 and is nearly independent of absolute deviatoric stress level. By contrast, the shear stress sensitivity increases from $\eta = -0.075$ at zero deviatoric stress to $\eta = -0.31$ at 55 MPa deviatoric stress. Negative η indicates a dilatant response to increased shear stress.

Similar results were obtained for the Navajo sandstone sample (Figure 5). Again, the mean stress sensitivity *B* = ~0.46 was nearly independent of deviatoric stress while the shear stress sensitivity increased systematically from $\eta = 0$ at zero deviatoric stress to $\eta = -0.21$ at 42 MPa deviatoric stress. The rapidly increasing first measurements (open circles) at $\sigma_d = 32$ and 42 MPa include progressively more inelastic dilatant deformation as the sample approached failure stress. In fact, there was sufficient time-dependent creep at $\sigma_d = 52$ MPa that attempts to measure elastic response were abandoned. The change in η with deviatoric stress was approximately $\partial\eta/\partial\sigma_d = -0.0009$ MPa^{-1} for Berea and $\partial\eta/\partial\sigma_d = -0.0013$ MPa^{-1} for the Navajo sample.

Two additional control tests were performed to check the validity of the preceding sandstone observations that $\eta \neq 0$ and that η became more negative with increasing deviatoric stress. First, since the sandstones have natural bedding, they show an inherent

anisotropy. Since standard poroelastic theory assumes an isotropic medium, we needed to test the importance of the initial sample anisotropy. We chose to test a sample composed of hand-packed Ottawa sand to assure an initially isotropic grain structure. This sample was tested following the same procedure as the sandstone samples with the exception that it was loaded in two cycles; first increasing σ_d to 15 MPa, unloading deviatoric stress and then reloading to $\sigma_d = 17.5$ MPa. As is typical for an unconsolidated, cohesionless sample the sand pack underwent considerable permanent deformation as well as a gradual strain hardening with application of increasing deviatoric stress.

Ottawa sand results are shown in Figure 6. Mean stress sensitivity B ranged from approximately 0.75 to 0.82 with only minor sensitivity to deviatoric stress level. This range of values is notably higher than the Skempton coefficient values measured for the sandstone and reflects the more compliant matrix and lack of cohesion of the sand pack. The most significant finding of the Ottawa sand measurements is the deviatoric stress dependence of η, ranging from approximately –0.13 at 5 MPa deviatoric stress to about –0.42 at 17.5 MPa. Thus, the initially isotropic sand pack, similar to the sandstone samples, shows an increased undrained pore pressure sensitivity to increasing deviatoric stress level. It is also interesting to note that the sand pack sample appears to retain memory of its past stress history. That is, the second cycle of loading shows a permanent offset in η relative to the values measured in the first loading cycle. This offset is probably a result of the cumulative, non-recoverable crack damage or grain size reduction that accompanies sample loading.

The final test sequence was carried out on a sample of porous ceramic (high-purity Al_2O_3). This is a fine-grained ceramic that has been partially fired to retain 42 percent porosity. Results are shown in Figure 7. Since the grains have small diameter and have been sintered, this material forms a relatively stiff matrix for such high porosity. Consequently, we obtain a low value of mean stress sensitivity of $B = 0.12$ which does not change as deviatoric stress level increases. In addition, this sample appears to have no deviatoric stress sensitivity ($\eta = +0.0036\pm0.0052$) at all applied deviatoric stress levels tested.

5. Discussion

5.1. Isotropic poroelastic response.

Measurements made under hydrostatic loading conditions ($\sigma_d = 0$) are consistent with earlier studies of undrained pore pressure response to changes in mean stress [*Hart and Wang*, 1995]. Namely, an increase in confining pressure leads to microcrack closure and matrix stiffening and therefore a steady decline in pore pressure response (Figure 3). This monotonic decrease in B is observed in sandstone samples as well as in the unconsolidated Ottawa sand pack. When deviatoric stress is applied to the samples (Figures 4 - 7), mean stress sensitivity, B, shows only a second order dependence on absolute deviatoric stress level.

The observed decline in B with increasing effective pressure can be related to changes in compressibility as suggested by *Zimmerman* [1991, pp. 62]. Using his nomenclature, Skempton's coefficient can be related to rock compressibility according to

$$B = \frac{\left(C_{pp} + C_r\right)}{\left(C_{pp} + C_f\right)} \tag{10}$$

where compressibilities are defined as follows: C_{pp} is compressibility of pore space in response to changes in pore pressure, C_r is compressibility of the rock matrix material and C_f is compressibility of the pore fluid (water). Zimmerman notes that in general, C_f is greater than C_r, implying bounds on Skempton's coefficient of $0 \leq B \leq 1$. In a test of the effective pressure law for sandstone compressibility, *Zimmerman et al.* [1986] reported drained compressibility measurements of Berea sandstone up to 40 MPa effective confining pressure. Using *Zimmerman et al.'s* [1986] compressibility measurements, $C_r = 0.26$ x 10^{-4} MPa^{-1} and water compressibility at $p = 3$ MPa of $C_f = 4.3$ x 10^{-4} MPa^{-1}, we can estimate Skempton's coefficient from equation (10). Results are plotted as the solid line in Figure 3. The observed and predicted curves have the same general shape and show an asymptotic pressure of about 40 MPa. However, the Zimmerman *et al.* [1986] compressibility data predict a smaller pressure sensitivity of B than is observed in the combined undrained Berea measurements of *Green and Wang* [1986] and this study. The high pressure asymptotic value of B predicted by equation (10) is 0.47 while our direct measurement is 0.4. This difference may be the result of differences in samples. Berea sandstone is known to vary in clay content, porosity and other characteristics. A proper test of (10) would involve undrained poroelastic measurements and compressibility measurements on the same sample.

5.2. Stress-induced anisotropic response.

What is clearly established in these experiments is that the undrained pore pressure response of porous sandstone as well as cohesionless sand is sensitive to deviatoric stress. The last term in equation (6) predicts that this sensitivity is related to the difference in compliance (related to $(m - h)$) between the axial and transverse directions in the test samples. We expect that with the application of axial load m will decrease more rapidly than h (in fact, h probably increases with increasing stress) and deviatoric stress sensitivity becomes more negative. This expectation is consistent with the measured response for the sandstones and sand pack. It is also responsible for the stress-induced anisotropy in both P- and S-wave velocities in samples subjected to deviatoric stress (see, for example [*Nur and Simmons*, 1969; *Bonner*, 1974; *Lockner et al.*, 1977; *Lockner et al.*, 1992]). Figure 8 shows the development of stress-induced anisotropy in P-wave velocity in a dry sample of Berea sandstone deformed at 50 MPa confining pressure. By 100 MPa deviatoric stress, a 16 percent anisotropy had developed between the axial and transverse P-wave speeds, due mainly to an increase in compliance in the transverse direction. Up to 140 MPa, the stress-induced anisotropy is mostly reversible since only minor new microcrack damage occurs below this stress level [*Lockner et al.*, 1992].

Using the formulation represented in (7), the deviatoric stress sensitivity of the undrained pore pressure response can be approximated by

$$\eta = \eta_o + q\sigma_d \ . \tag{11}$$

For all of the samples tested we find $-0.075 \leq \eta_o \leq 0$. For the porous ceramic sample $q = 0$. For all other samples q is negative. At the 17 MPa effective confining pressure used in these experiments, sandstone samples show values of $q = -0.003$ and -0.005 MPa^{-1}. The Ottawa sand sample yields $q \sim -0.018$ MPa^{-1}. Normalizing deviatoric stress by peak strength would bring these values of q for the sandstones and the Ottawa sand closer together. However, more experiments are needed to determine if this normalization would provide a general improvement in consistency for different sample types under different stress conditions.

In Section 2 we postulated that the undrained pore pressure response can be decomposed, as represented by (7), into independent factors related to mean stress and deviatoric or shear stress. In addition to measuring η and B separately, we carried out additional tests that can be used to provide some measure of the validity of (7). This additional set of tests involved changing deviatoric stress at constant confining pressure so that deviatoric and mean stress varied in the ratio $\Delta\sigma_s/\Delta\sigma_m = 3/2$. A predicted pore pressure response, based on (7) and using the observed values of η and B under the given test conditions, was computed for the various deviatoric stress tests. A comparison of the observed versus predicted pore pressure response is shown in Figure 9 for the sandstone and Ottawa sand experiments (at all ambient deviatoric stress levels). Since B is nearly independent of deviatoric stress and η becomes more negative with deviatoric stress, values plotting close to the origin represent measurements at higher deviatoric stress levels. If (7) is a valid representation of the undrained pore pressure response, then, within experimental error, points in Figure 9 would fall on a line of slope equal to 1 and passing through the origin. Predictions for the same data set using observed values of B alone (*i.e.,* equation (1)) are plotted using smaller symbols ('+', 'x' and 'o') in Figure 9. Although equation (7) does not provide a perfect fit to the observations, it represents a significant improvement over the predictions based on mean stress changes alone.

The undrained poroelastic response presented here for sandstone is consistent with Biot theory for an initially isotropic rock that becomes increasingly anisotropic due to the application of deviatoric stress. In this case, η is approximately zero under hydrostatic stress conditions and becomes increasingly negative as the sample is loaded towards failure. For loading less than about 50 percent failure stress, little new crack damage is sustained by the sample. In this case, when the sample is unloaded, anisotropy should disappear and η should return to zero. Above approximately 50 percent of peak stress, deviatoric stress induces the growth of new microcracks. Yet at all stress levels, the strain response of a rock can be partitioned between reversible opening and closing of existing cracks and irreversible growth of new cracks or extension of existing cracks. Since we observe changes in η below 50 percent peak stress, we suggest that the linear dependence of η on deviatoric stress level is the poroelastic response of existing cracks. The curvature in η for the Berea samples above 50 MPa (Figure 4) may reflect the addition of a significant number of new microcracks as the stress level approaches peak stress. It should be noted that all of these arguments can be applied to the stress dependence of P-wave velocity anisotropy as shown in Figure 8. In fact, there should be a close connection between stress-related changes in P-wave velocity and variations in η and B.

We propose that the observed stress dependence of η is related to preferential closure of elongated pores or thin, low-aspect-ratio cracks in the sandstone and Ottawa sand

samples as well as to the change in area of grain contacts. When deviatoric stress is first applied at constant mean stress, flat cracks normal to the maximum compressive stress direction will tend to close (see, for example, [*Pollard and Segall*, 1987; *Zimmerman*, 1991]). To maintain constant mean stress, an increase in σ_1 implies a decrease in σ_2 and/or σ_3. Thus cracks parallel to σ_1 will tend to open. For an isotropic material including cracks of all orientations, cracks that open and cracks that close will, to first order, balance and the net pore volume change will be zero (implying $\eta \sim 0$). However, as the ambient deviatoric stress level increases, more and more cracks normal to σ_1 are forced closed. Once these cracks close, they can no longer contribute to a reduction in pore space. (This effect is observed in the decrease in stress sensitivity of the fast P-wave velocity with the progressive application of deviatoric stress (*e.g.*, [*Lockner et al.*, 1977; *Lockner et al.*, 1992] and Figure 8). Since cracks parallel to σ_1 continue to open in response to the drop in σ_2 and σ_3, the reversible pore volume response to an increase in deviatoric stress becomes progressively more dilatant. This is precisely the effect observed in our experiments. Since this process is reversible, complete unloading of deviatoric stress should allow closed microcracks to open and the poroelastic response at near-zero deviatoric stress should again give $\eta \sim 0$. Thus, the anisotropic poroelastic response is expected to be the result of stress induced, but reversible, crack anisotropy.

A second mechanism which is likely to operate in porous sandstones involves the change in grain contact area in response to applied load. As load increases, grain contacts deform and contact area increases, reducing the compliance of the rock matrix. Under deviatoric stress conditions, this stiffening effect can also lead to stress-induced anisotropy in the rock as expressed by equation (6).

According to this model, the offset in η in the Ottawa sand between the first and second cycles would be due to a permanent crack anisotropy induced by the finite and permanent axial shortening and grain crushing under the applied deviatoric stress field. The sandstone samples, by contrast, were not stressed to the point where a significant amount of permanent damage had occurred. The porous ceramic represents what might be termed the classic Biot response. Since this sample was sintered, grain contacts have been welded and pores have become nearly equant. Unlike the sandstones, the ceramic sample contains few low-aspect-ratio microcracks. Since round pores provide the greatest resistance to stress-induced pore collapse [*Zimmerman*, 1991], the ceramic sample most closely approximates the pore response assumed in the isotropic Biot model. The round pores will never completely close with the application of deviatoric stress and the stress sensitivity of pore pressure for this sample is zero at all stress levels.

5.3. Application to faults in the Earth.

There has been considerable interest recently in the question of earthquake interactions by the transfer of stresses [*Stein et al.*, 1992; *Simpson and Reasenberg*, 1994; *Harris et al.*, 1995; *Harris*, 1998; *Stein*, 1999]. When rupture of one fault induces a stress change on a neighboring fault, the parameter most commonly used to infer whether the second fault has been brought closer to failure is the change in Coulomb failure stress

$$\Delta\sigma_c = \Delta\tau_r - \mu\left(\Delta\sigma_n - \Delta p\right) \tag{12}$$

where $\Delta\tau_r$ is change in shear stress on the target fault plane in the expected rake (slip) direction, $\Delta\sigma_n$ is the change in normal stress and μ is coefficient of friction. Equation (12) assumes that an increase in shear stress moves a fault closer to failure while an increase in effective normal stress ($\sigma_{n,eff} = \sigma_n - p$) moves the fault away from failure. Most calculations of stress transfer following earthquakes either neglect poroelastic effects or incorporate them in what is termed an apparent coefficient of friction [*Beeler et al.*, 2000]. In more recent calculations that attempt to treat poroelastic effects in a more rigorous manner [*Beeler et al.*, 2000; *Cocco and Rice*, 2002], undrained pore pressure response is determined using the standard Skempton coefficient *B* and the coupling relation (1).

The addition of a shear stress dependence of pore pressure can be expected, under most circumstances, to have a stabilizing influence. This was found by *Wang* [1997] where he noted that the addition of a shear stress dependent pore pressure response tended to increase the areal extent over which pore pressure decreases occurred. The reason for this stabilizing effect is that for negative η, as measured for sandstone and Ottawa sand in our experiments, an increase in shear stress becomes coupled with an increase in effective normal stress. This effect is shown if Figure 10 where we have made Mohr representations of the stress changes associated with two representative stress steps. In Figure 10a (curve *i*) we show the change in stress state for faults whose normals are in the σ_1-σ_3 plane when σ_1 is increased by 1 MPa and there is no accompanying pore pressure change. This might represent the stress change due to tectonic loading in a reverse faulting regime. The horizontal axis represents change in effective normal stress and contours of changes in Coulomb failure stress (assuming μ = 0.6) are indicated by dashed lines. All stress states above and to the left of $\Delta\sigma_c = 0$ have been moved closer to failure while stress states below and to the right of $\Delta\sigma_c = 0$ have been moved away from failure. In the absence of pore pressure effects, the increase in σ_1 has stabilized some fault orientations (those whose normals are near the σ_1 direction) by increasing normal stress. Most fault orientations, however, have been destabilized by increasing shear stress. Curve *ii* in Figure 10a shows the effect of adding the standard undrained poroelastic response with *B* = 0.5. Since the increase in σ_1 has caused a 0.33 MPa increase in σ_m, pore pressure has increased and $\sigma_{n,eff}$ is reduced. This is the well-known destabilizing effect of increasing pore pressure in an isolated fault. Curve *iii* shows the effect of adding both *B* = 0.5 and η = -0.24. Since the increase in σ_1 has also increased σ_d, pore pressure is reduced so that the pore pressure change due to increasing σ_m is nearly canceled by the response to increasing deviatoric stress.

The second representative case, shown in Figure 10b, is for a 1 MPa decrease in σ_3. This case might represent tectonic loading in an extensional regime. Note that for curve *i*, all fault orientations have been destabilized, by a combined reduction in normal stress and increase in shear stress. For *B* = 0.5 (curve *ii*), the reduction in σ_m reduces pore pressure and increases effective normal stress. With *B* = 0.5 and η = -0.24 (curve *iii*), increasing σ_d further reduces pore pressure and increases $\sigma_{n,eff}$. Thus, in this case both the mean stress and deviatoric stress dependence of pore pressure tend to reduce the destabilizing effect caused by decreasing σ_3.

One final comment is worth noting regarding the stabilizing effect of $\eta < 0$. These experiments and associated analysis were carried out for axisymmetric loading of

samples with $\sigma_1 > \sigma_2 = \sigma_3$. Using the same analysis, η greater than zero would occur by making the intermediate principal stress equal to the maximum principal stress; that is, for $\sigma_1 = \sigma_2 > \sigma_3$. In this case, increasing deviatoric stress would act to increase pore pressure and destabilize a fault system. The present analysis is restricted to axisymmetric stress states. A more generalized analysis would seem useful in determining the conditions under which poroelastic effects can lead to fault destabilization.

6. Conclusions

In this study we have measured the undrained pore pressure response of sandstones and quartz sand to changes in mean stress and deviatoric stress. Since standard poroelastic theory for isotropic media predicts that undrained pore pressure response should be insensitive to changes in deviatoric stress, little attention has been paid to the measurement of poroelastic response in rock near failure. Our observations confirm that the standard mean-stress-dependent Skempton coefficient *B* is, to first order, independent of applied deviatoric stress level. The more noteworthy result is that both sandstone samples and the Ottawa sand sample showed a dependence of pore pressure on changes in deviatoric stress. At high deviatoric stress levels, the undrained pore pressure response, due to changes in pore volume, included components of both elastic and inelastic strain. By repeated stress cycling, the inelastic response was eliminated and the reversible elastic component could be measured directly. The deviatoric stress sensitivity of pore pressure, measured at constant mean stress, was found to increase with increasing deviatoric stress level. Since the pore volume increased with increasing deviatoric stress in these rocks, the resulting drop in pore pressure would have a stabilizing effect on the rock.

The poroelastic response to deviatoric stress reported here appears to be the result of stress-induced anisotropy. If stress cycling is limited to a region where no significant new microcrack damage occurs, then the poroelastic response is reversible and the coefficient η varies linearly with applied stress level. Upon unloading, the rock will revert to a nearly isotropic state and the coefficient η will approach zero. A direct comparison can be made to stress-induced wave-speed anisotropy which responds to the opening and closing of microcracks in a rock matrix when loaded in a non-hydrostatic stress state.

This deviatoric-stress-dependent poroelastic response has now been observed in limestone, sandstone and Ottawa sand. If this property is common in porous rock, it suggests that many previous calculations of poroelastic response, especially at high deviatoric stress, have neglected an important term in the basic constitutive relations.

References

Beeler, N.M., R.W. Simpson, S.H. Hickman, and D.A. Lockner, Pore fluid pressure, apparent friction, and Coulomb failure, *J. Geophys. Res.*, *105* (B11), 25,533-25,542, 2000.

Biot, M.A., General theory of three dimensional consolidation, *J. Appl. Phys.*, *12*, 155-164, 1941.

Biot, M.A., Theory of elasticity and consolidation for a porous anisotropic solid, *J. Appl. Phys.*, *26* (2), 182-185, 1955.

Biot, M.A., and D.G. Willis, The elastic coefficients of the theory of consolidation, *J. Appl. Mech., Trans. ASME*, *79*, 596-601, 1957.

Bonner, B.P., Shear wave birefringence in dilating granite, *Geophys. Res. Lett.*, *1* (5), 217-220, 1974.

Cheng, A.H.-D., Material coefficients of anisotropic poroelasticity, *Int. J. Rock Mech. Min. Sci. Geomech. Abstr.*, *34* (2), 199-205, 1997.

Cocco, M., and J.R. Rice, Pore pressure and poroelasticity effects in Coulomb stress analysis of earthquake interactions, *J. Geophys. Res.*, *107*, 2002 in press.

Green, D.H., and H.F. Wang, Fluid pressure response to undrained compression in saturated sedimentary rock, *Geophysics*, *51*, 948-956, 1986.

Harris, R.A., Introduction to special section: Stress triggers, stress shadows, and implications for seismic hazard, *J. Geophys. Res.*, *103*, 347-358, 1998.

Harris, R.A., R.W. Simpson, and P.A. Reasenberg, Influence of static stress changes on earthquake locations in southern California, *Nature*, *375*, 221-224, 1995.

Hart, D.J., and H.F. Wang, Laboratory measurements of a complete set of poroelastic moduli for Berea sandstone and Indiana limestone, *J. Geophys. Res.*, *100*, 17,741-17,751, 1995.

Henkel, D.J., and N.H. Wade, Plane strain tests on a saturated remoulded clay, *J. Soil Mech. Found. Div. Am. Soc. Civ. Eng.*, *92(SM6)*, 67-80, 1966.

Jaeger, J.C., and N.G.W. Cook, *Fundamentals of Rock Mechanics*, 593 pp., Chapman and Hall, New York, 1984.

Lockner, D.A., J.D. Byerlee, V. Kuksenko, A. Ponomarev, and A. Sidorin, Observations of quasistatic fault growth from acoustic emissions, in *Fault Mechanics and Transport Properties of Rocks*, edited by B. Evans, and T.-f. Wong, pp. 3-31, Academic Press, London, 1992.

Lockner, D.A., J.B. Walsh, and J.D. Byerlee, Changes in seismic velocity and attenuation during deformation of granite, *J. Geophys. Res.*, *82* (33), 5374-5378, 1977.

Nur, A., and G. Simmons, Stress-induced velocity anisotropy in rock: An experimental Study, *J. Geophys. Res.*, *74* (27), 6667-6674, 1969.

Pollard, D.D., and P. Segall, Theoretical displacements and stresses near fractures in rock: with applications to faults, joints, veins, dikes, and solution surfaces, in *Fracture Mechanics of Rock*, edited by B.K. Atkinson, pp. 277-349, Academic Press, New York, 1987.

Rice, J.R., and M.P. Cleary, Some basic stress diffusion solutions for fluid-saturated elastic porous media with compressible constituents, *Rev. Geophys. and Space Phys.*, *14* (2), 227-241, 1976.

Roeloffs, E., Poroelastic techniques in the study of earthquake related hydrologic phenomena, *Adv. Geophys.*, *37*, 135-195, 1996.

Simpson, R.W., and P.A. Reasenberg, Earthquake-induced static stress changes on Central California faults, in *The Loma Prieta, California Earthquake of October 17, 1989 - Tectonic Processes and Models*, edited by R.W. Simpson, pp. F55-F89, U.S. Geol. Surv. Prof. Pap., 1550-F, 1994.

Skempton, A.W., The pore-pressure coefficients A and B, *Geotechnique*, *4*, 143-147, 1954.

Stein, R., G.C.P. King, and J. Lin, Change in failure stress on the southern San Andreas fault system caused by the 1992 magnitude = 7.4 Landers earthquake, *Science*, *258*, 1328-1332, 1992.

Stein, R.S., The role of stress transfer in earthquake occurrence, *Nature*, *402*, 605-609, 1999.

Wang, H.F., Effects of deviatoric stress on undrained pore pressure response to fault slip, *J. Geophys. Res.*, *102*, 17,943-17,950, 1997.

Zimmerman, R.W., *Compressibility of sandstones*, 173 pp., Elsevier, Amsterdam, 1991.

Zimmerman, R.W., W.H. Somerton, and M.S. King, Compressibility of porous rocks, *J. Geophys. Res.*, *91* (B12), 12,765-12,777, 1986.

Table 1

Sample	length mm	porosity %	grain size mm	hydrostatic test $P_{c,eff}$, MPa	deviatoric stress test σ_d (at $P_{c,eff}$=17MPa)
Berea1	63.5	21	0.17	8, 17, 37	5 to 55
Berea2	63.5	21	0.17		0 to 35
Navajo	50.8	22	0.15	8, 17, 37	0 to 45
Ottawa sand	63.5	41	0.09	17, 37	0 to 17.5
Porous Ceramic	25.4	42			5 to 60
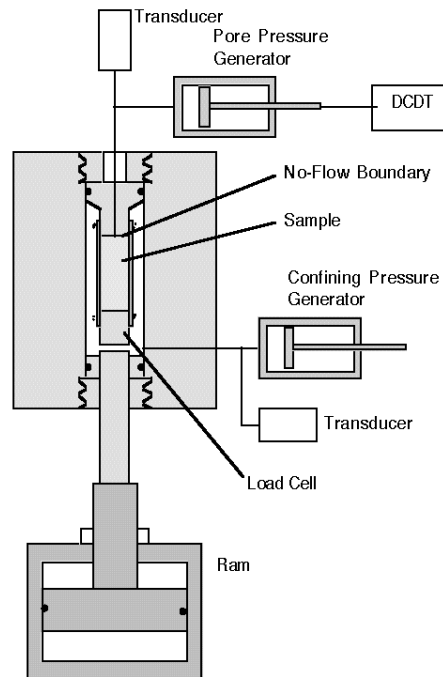
Figure 1. Schematic diagram of triaxial test geometry used to determine poroelastic constants under deviatoric stress conditions. External pore pressure generator was computer controlled to maintain a no-flow boundary condition at the top surface of the sample (see text).
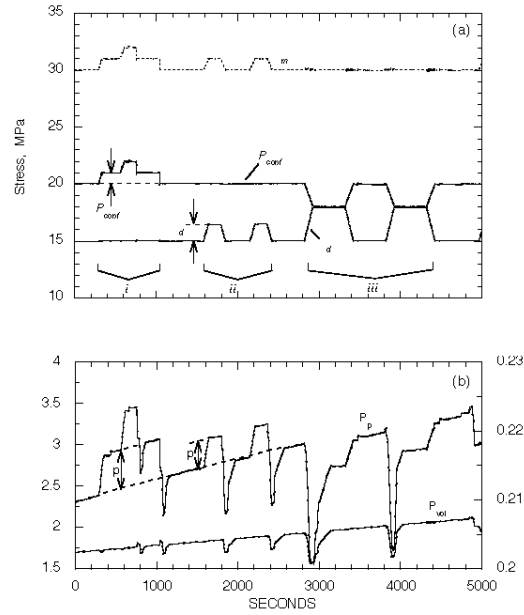
Figure 2. Example of test sequence used to measure poroelastic coefficients. (a) Time history of deviatoric stress (upper) and confining pressure (lower) showing three test segments. In segment *i*, confining pressure and axial stress were varied together while maintaining constant deviatoric stress. This test determined *B*. In segment *ii*, deviatoric stress was cycled at constant confining pressure. In segment *iii*, deviatoric stress and confining pressure were varied to maintain constant mean stress. This test determined

η (equation (7)). (b) Pore pressure response to stress steps shown in upper plot. Undershoots at beginnings of downward pressure steps were manually induced to eliminate backlash errors in the pore volume measurements (see text). Lower curve is the pore volume channel showing the flux of water into or out of the sample. The slow increase in pore volume, reflected in the gradual increase in pore pressure, was used to reduce measurement errors (see text).

Skempton Coefficient (Hydrostatic Stress)
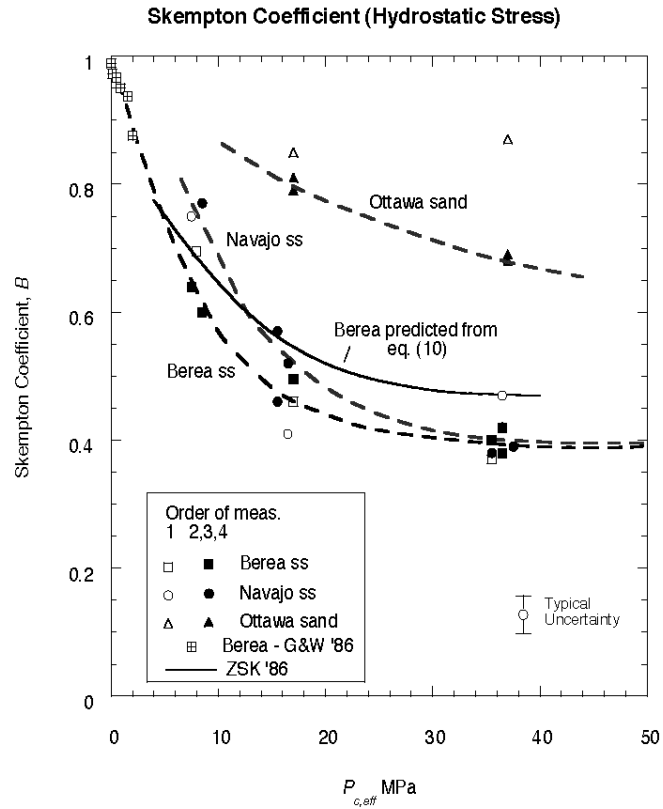
Figure 3. Plot of Skempton coefficient *B* as a function of effective confining pressure ($P_{c,eff} = P_c - p$). The sandstones show similar response while the cohesionless Ottawa sand has a significantly larger coefficient. All samples show a decrease in pore pressure response with increasing confining pressure due to increased matrix stiffening. Low pressure Berea data after *Green and Wang* [1986]. Also plotted is *B* predicted from

compressibility data of Berea measured by *Zimmerman et al.* [1986] and using equation (10) (see Section 5.1).
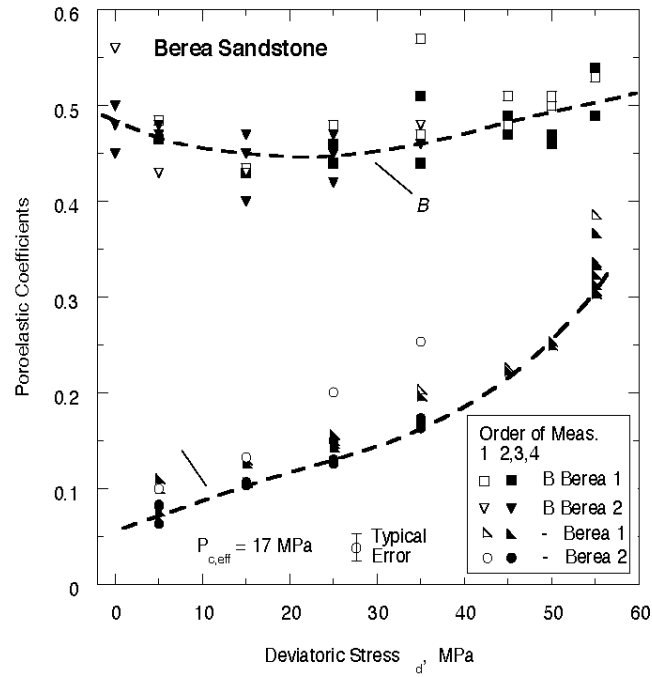
Figure 4. Poroelastic constants *B* and -η plotted versus deviatoric stress for two Berea sandstone samples. Peak strength at this confining pressure is σ_d =65 MPa. Open symbols

are for first loading cycle which, especially at higher stress levels, includes a portion of irreversible pore volume change. Solid symbols are for repeated stress cycles which measure the reversible (elastic) pore pressure response. *B* (upper curve) shows little change with deviatoric stress level. Deviatoric stress dependence, plotted as -η (lower curve), increases approximately linearly with increasing deviatoric stress level.
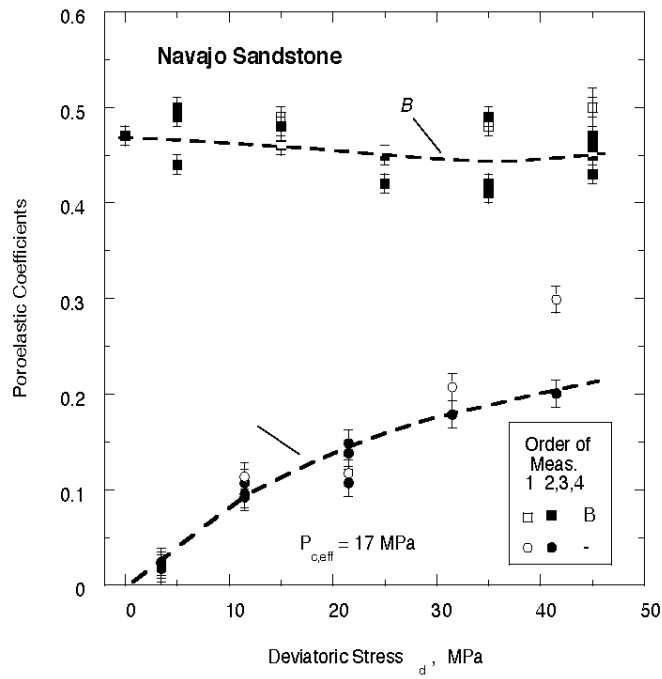
Figure 5. Poroelastic constants *B* and -η plotted versus deviatoric stress for Navajo sandstone sample. Similar to Berea sandstone, deviatoric stress dependence increases with increasing stress level.
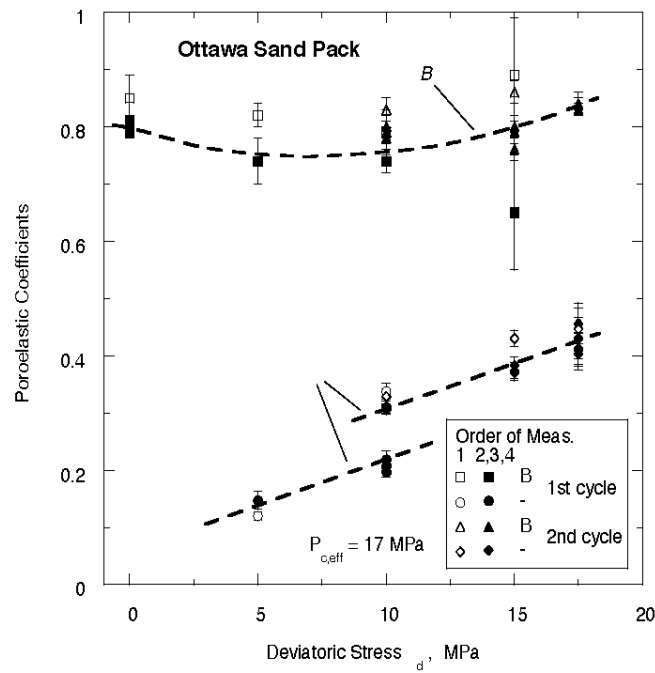
Figure 6. Poroelastic constants *B* and -η plotted versus deviatoric stress for crushed Ottawa sand pack. Sample was loaded to σ_d = 15 MPa, unloaded, and then reloaded to 17.5 MPa. Stress cycling apparently resulted in an offset in the shear-stress-dependent response.
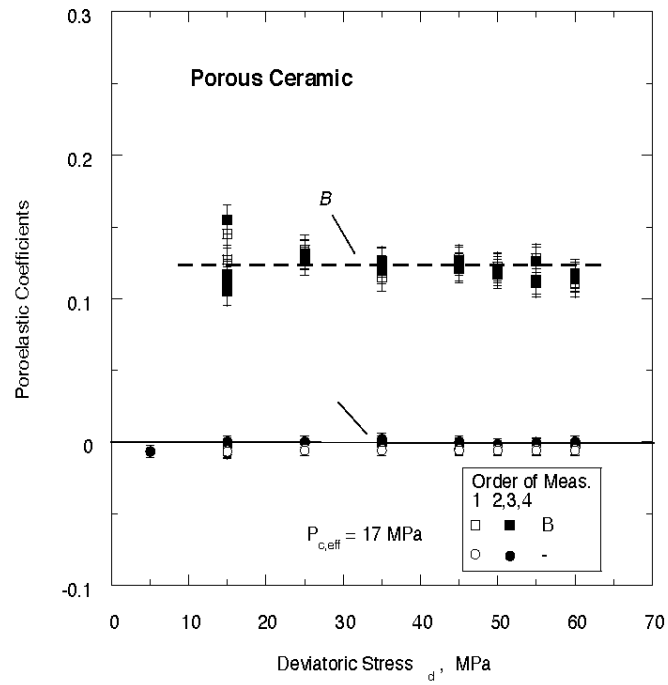
Figure 7. Poroelastic constants *B* and -η plotted versus deviatoric stress for a control sample of sintered, porous ceramic. This fine-grained sample had a much lower Skempton coefficient *B* than the sandstone or Ottawa sand samples. In addition, the deviatoric stress sensitivity was zero at all stress levels.
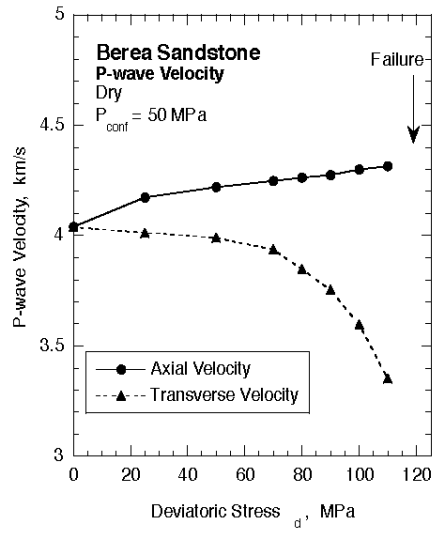
Figure 8. Plot of fast (axial) and slow (transverse) P-wave velocities in a Berea sandstone sample loaded to failure at 50 MPa confining pressure (sample S2 from [*Lockner et al.*, 1992]). Stress-induced velocity anisotropy reflects a systematic change in stiffness moduli within the sample and through equation (6) implies changes in the poroelastic response.
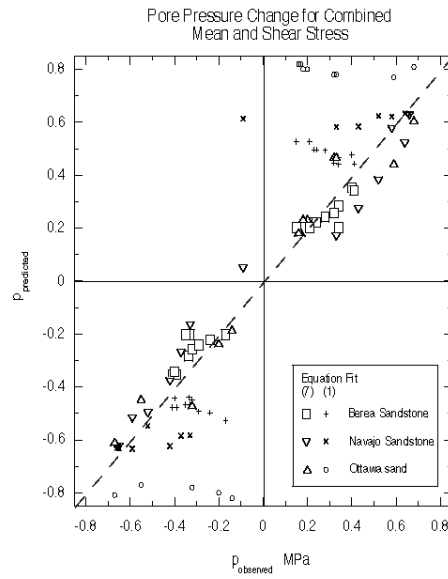
Figure 9. Plot of predicted pore pressure response (based on equation (7)) versus observed response for sandstones and Ottawa sand samples. Measurements at high deviatoric stress are near the origin. Small symbols ('+', 'x', and 'o') show predicted response based on Skempton coefficient alone (equation (1)).
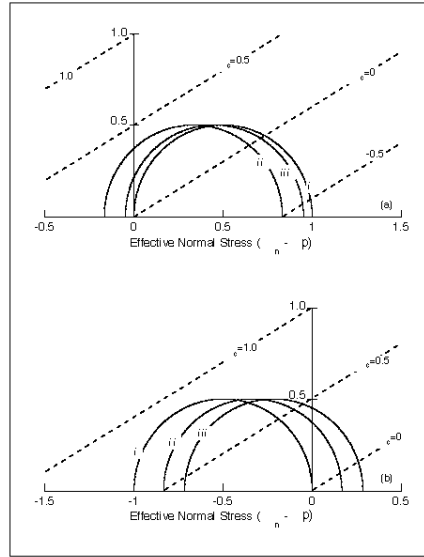
Figure 10. Changes in shear versus effective normal stress plots for two representative stress changes showing the effect of undrained poroelastic response. Circles are representations of stress states on planes whose normals are in the σ_1-σ_3 plane. (a) Change in stress state due to a 1 MPa increase in σ_1. (b) Change in stress state due to a 1 MPa decrease in σ_3. Curve *i*: $B = \eta = 0$. Curve *ii*: $B = 0.5$, $\eta = 0$. Curve *iii*: $B = 0.5$, $\eta = -$

0.24. Stress states in regions of increased $\Delta\sigma_c$ have moved closer to failure. Deviatoric stress dependence of pore pressure tends to stabilize faults in both examples.